Draft version October 7, 2022
Typeset using LaTeX **twocolumn** style in AASTeX631

Observation of HD 189733 b Exoplanet Transit

112166935,[1] 112601517,[1] and 112695826[1]

[1] *Department of Physics and Astronomy*
Stony Brook University
Stony Brook, NY 11794, USA

ABSTRACT

We conducted optical imaging observations of a transit of the exoplanet HD 189733 b. The observations occurred on the night of 2022-08-31 to 2022-09-01 at Mount Stony Brook Observatory, Stony Brook University, Stony Brook, NY 11794, USA. We used the B-band filter for our telescope. We measured a transit depth of $2.35 \pm 0.17\%$ and a transit duration of 1.68 ± 0.24 hours. The transit was observed to begin on 2022-08-31 22:48 and end on 2022-09-01 00:29.

Keywords: Optical Astronomy (1) — Exoplanet (2) — Transit (3) — Imaging (4)

1. INTRODUCTION

Extrasolar planets, also known as exoplanets, are planets that orbit stars other than the Sun. Exoplanets have been discovered and studied using a variety of techniques, such as radial velocity, transit, and direct imaging. HD 189733 b is a frequently studied exoplanet due to its host star brightness and large transit depth (Cauley et al. 2017).

In this lab we observed a transit of the exoplanet HD 189733 b through a B-band filter. Using a CCD, we collected light from the source star, HD 189733, as well as neighboring stars. We processed and plotted the photometric data as a lightcurve to show the characteristic transit. From the transit lightcurve, we calculated the transit depth. We calculated other properties of the exoplanet, namely planet-to-star radius ratio and transit duration. The purpose of this lab was to confirm the transit of HD 189733 b predicted to occur on the night of 2022-08-31 22:54 to 2022-09-01 00:40 local Mean Solar Time (ipa 2022), and to measure the transit depth cited to be 2.4% (Cauley et al. 2017).

2. SOURCE SELECTION

We select HD 189733 as our star and HD 189733 b as our exoplanet. We gather preliminary data about our star and planet from the SIMBAD and exoplanet.eu catalogs, such as coordinates, magnitude, and transit date. Using the coordinates of the star, we obtain a finder chart from AAVSO (Figure 1) and an object altitude chart from StarAlt (Figure 2) in order to plan our observation. We used the Transit Predictor Tool from Caltech (ipa 2022) to determine the observation date and times. We selected 2022-08-31 to 2022-09-01 as our observation date.

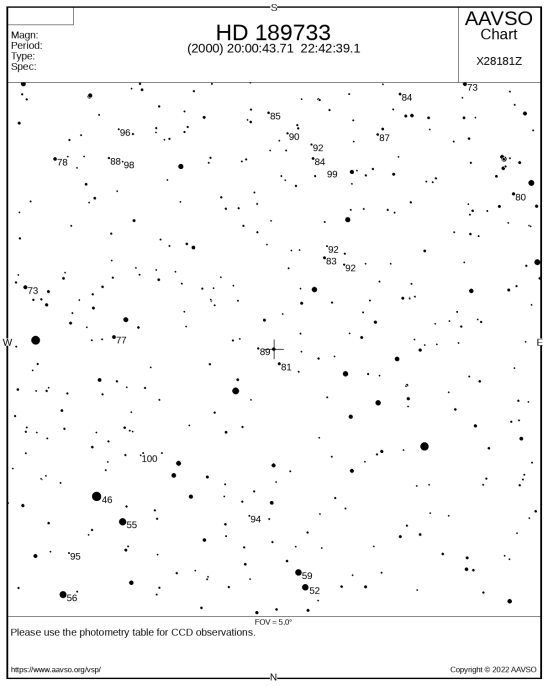

Figure 1. 5° Finding chart for HD 189733

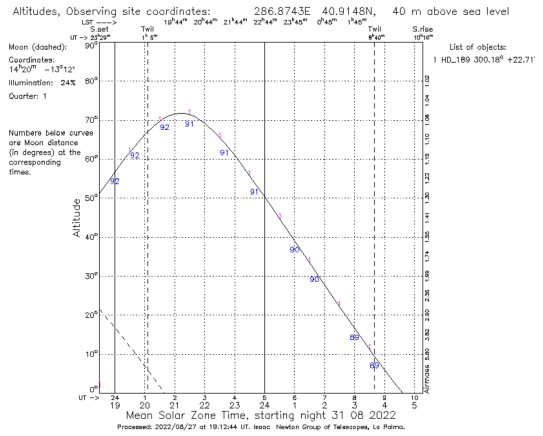

Figure 2. Altitude chart for HD 189733 on 2022-08-31

3. DATA ACQUISITION (PROCEDURE)

We conducted our observations on the night of 2022-08-31 21:58 to 2022-09-01 01:59. Our target culminated at approximately 21:00 local Mean Solar Time. We ended our observations at approximately 2022-09-01 02:00, when our target star altitude dipped below 30°, when high airmass produces atmospheric seeing effects that would add statistical error to flux measurements (von der Linden, Anja (2022a), von der Linden, Anja (2022b)). We used the Mount Stony Brook Observatory, on the rooftop of the Earth and Space Sciences building at Stony Brook University. The observing night was clear and somewhat windy. We opened the doors and dome hatch to mitigate atmospheric seeing. (von der Linden, Anja 2022c)

We connected our CCD to the telescope, powered on the CCD and telescope, and loaded up the Cartes du Ciel software on the Astronomy lab laptop. After performing a meridian flip of the telescope, we guided it to our target star using Cartes du Ciel and the hand pad. Upon identifying our star, we set the telescope to track the star and focused the camera to obtain clear images of the star field.

We took test exposures such that our brightest star (also our target star) showed between 20,000 and 30,000 counts in its brightest pixel. We took 10 flat fields of the dome wall when it was uniformly lit, all with the same exposure time. Throughout the night, the camera took exposures and saved each science image automatically to the laptop. For each exposure time we used for science images, we took 10 dark frames.

In the middle of our observations, we encountered technical difficulties. One of our raw science images exhibited streaking behavior, indicating that the telescope was drifting rather than tracking the star properly. After we got the telescope to track our star again, we continued taking exposures.

At the end of the night, we transferred our darks, flats, and science images from the laptop to our personal devices, so that we could later perform data reduction and analysis. 602 of our 606 raw science images were used in our data analysis.

4. DATA REDUCTION

We used 3 exposure times in our observations: 10s, 12s, 20s. We took 10 dark frames for each of these exposure times, and generated a master dark frame for each exposure time by taking the median of the 10 dark frames. Taking the median dark frame yields a "typical" pixel reading (and hence dark current) that excludes outliers. From our master dark frames we can identify hot pixels.

We took 10 flat fields with constant exposure time. We calculated the master flat by taking the median of the flat fields and dividing by its mode. This rescales each pixel to a value between 0 and 1, indicating the relative sensitivity of each pixel. For example, we found that the center of the image was more sensitive than the edges of the image, and that certain pixels had reduced sensitivity due to dust grains interfering with light.

We used our master flat and master dark frames to calibrate our raw science images. We subtracted the master darks from the science images with the corresponding exposure times. Then we divided each dark-adjusted science image by the master flat to obtain calibrated science images.

We ran astrometry.net to solve each of our calibrated science images, yielding a coordinate for every pixel. We ran Source Extractor on our astrometrically solved science images to produce catalog files with star coordinates and flux counts.

From our calibrated science images, we extracted flux and flux error from the corresponding catalog file based on the statistics of pixel counts in a constant region drawn around our target star. We used the Tycho catalog to select our 10 reference stars, and we extracted each reference star's flux and flux error based on their coordinates. We constructed our flux table by dividing each image's star flux value and flux error by the image's exposure time. We extracted observation dates from raw science images and converted them to Python datetime objects. We appended each image's flux, flux error, and observation date to a CSV file.

4.1. *Lightcurves of reference stars*

We normalized each flux table value by the mean flux and converted each observation date to a mean julian

date (MJD) float value. We plotted the relative flux values (with flux error bars) with respect to MJD (Figure 3). From our reference star lightcurves, we observed that their flux tended to decrease and become more scattered later in the night. This is because our observed sky region was becoming lower in the sky, and hence atmospheric seeing effects tended to increase over time. We accounted for this effect in our target star flux values as follows:

We binned the data 10 points at a time to obtain the final lightcurve of our exoplanet transit (Figure 4, 5). Each bin in Figure 5 contains 10 data points. The value of each point in the binned lightcurve is the average of its bin, and the uncertainty of each point is the standard deviation of its bin.

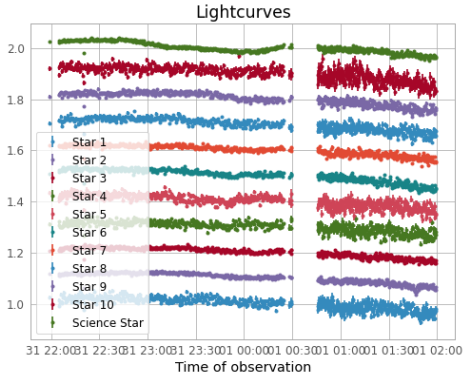

Figure 3. Lightcurves of reference stars and target star, with varying vertical offsets

5. RESULTS

Upon data reduction, we obtain raw and binned transit lightcurves for HD 189733 b.

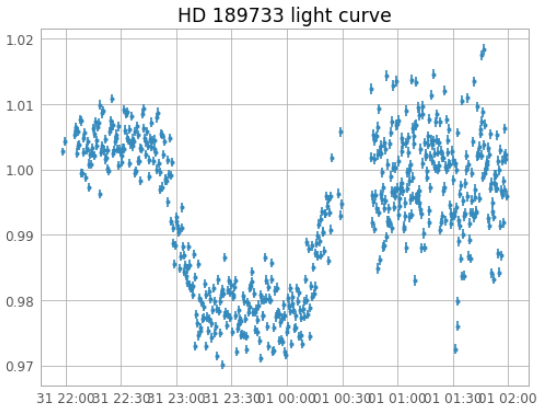

Figure 4. Unbinned transit lightcurve of HD 189733 b

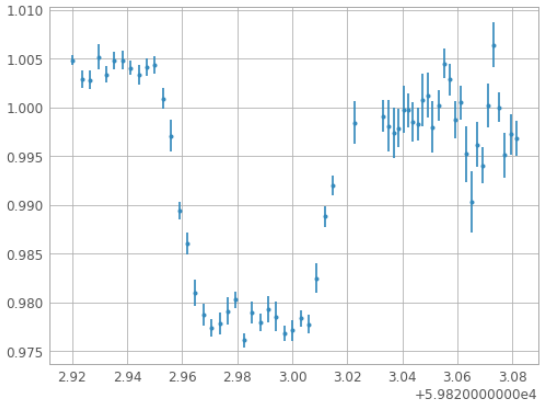

Figure 5. Binned transit lightcurve of HD 189733 b

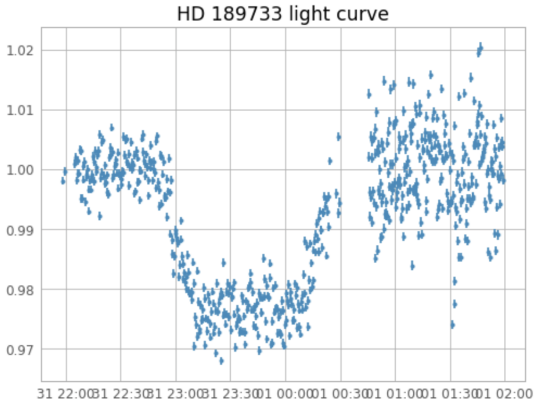

Figure 6. Unbinned transit lightcurve of HD 189733 b, adjusted for decreasing linear trend of data

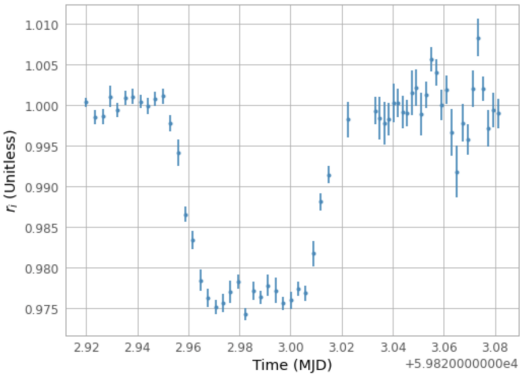

Figure 7. Binned transit lightcurve of HD 189733 b, adjusted for decreasing linear trend of data

6. ANALYSIS AND DISCUSSION

6.1. *Baseline Flux*

The flux of HD 189733 is markedly different after the transit than before the transit. Namely, HD 189733 is dimmer after its transit than before its transit. A pos-

sible explanation for this observation is that HD 189733 is a variable star of the type BY Draconis (SIM 2022). We correct for this variation in baseline flux by fitting a straight line to our data, then dividing by the straight-line fit. After correcting for the linear trend of the data, we obtain the variation-adjusted raw and binned lightcurve data for HD 189733 b in Figures 6 and 7.

6.2. *Transit Detection*

Qualitatively, the transit lightcurve of HD 189733 b agrees with expectation. We expect a dip in the relative flux of the star HD 189733 as HD 189733 b transits, which is what we observe.

We calculated the unweighted means of the binned data in the 3 time intervals in our data: before transit, during transit, after transit. We determined the mean pre-transit flux, denoted $f_{0,binned} = 1.0001 \pm 0.0009$, the mean post-transit flux, denoted $f_{2,binned} = 1.0001 \pm 0.0012$, and the mean during-transit flux, denoted $f_{1,binned} = 0.9766 \pm 0.0015$. We calculated the transit depth δ using Equation A5 and the uncertainty σ_δ using Equation A6 and obtain $\delta = 0.0235 = 2.35 \pm 0.0017\%$.

If our star has a flux of 0.9766 ± 0.0017 during transit, and a baseline flux of 1.0001, the significance of our transit is 13.82σ A9. This exceeds the 3σ detection threshold (von der Linden, Anja 2022b), so we successfully detected a transit of HD 189733 b.

With our measured transit depth of $2.35 \pm 0.17\%$ and an accepted transit depth of 2.40% (Cauley et al. 2017), we calculate a significance of 0.29σ (Equation A9) with respect to literature, which is less than 3σ. Hence our measurement of transit depth agrees with literature.

6.3. *Planet Radius*

Based on our transit depth of 2.35%, we calculate the planet-to-star radius ratio as 0.153 (Equation A7). We calculate the uncertainty in our planet-to-star radius ratio as 0.006 (A8). Therefore, our planet-to-star radius ratio is 0.153 ± 0.006. The radius ratio from literature is 0.155 (Sing, D. K. et al. 2009), so our planet-to-star radius ratio measurement has a significance of 0.33σ (Equation A9).

Our calculated planet-to-star radius ratio is 0.153 ± 0.006, and the literature planet-to-star radius radio is 0.155, yielding a significance of 0.33σ. Our significance is less than 3σ, so our planet-to-star radius ratio agrees with literature.

6.4. *Transit Duration*

By inspection of binned transit lightcurve data, we determine that the transit for HD 189733 b occurs from MJD $2.95+5.982\times10^4 = 59822.95$ to $3.02+5.982\times10^4 = 59823.02$, yielding a duration of 0.07 days. Converted to ISO time, our transit occurred from 2022-08-31 22:48 to 2022-09-01 00:29, which agrees with the predicted transit time of 2022-08-31 22:54 to 2022-09-01 00:40.

Our transit duration is 0.07 days, and its uncertainty is about 0.01 days. Therefore, our measurement of transit duration is 0.07 ± 0.01 days, or 1.68 ± 0.24 hours. The accepted transit duration of HD 189733 b is 1.827 ± 0.029 hours (Winn et al. 2007). The significance of our transit duration is 0.68σ (Equation A9), so our transit duration agrees with the literature.

7. CONCLUSION

We observed a transit of HD 189733 b. Our transit depth was calculated as $2.35 \pm 0.17\%$ and determined to be a significant detection. Our transit depth agrees with the accepted transit depth of 2.40%. From our transit depth measurement we calculated the planet-to-star radius ratio as 0.153 ± 0.006, which agrees with the accepted radius ratio of 0.155. Our measured transit duration of 1.68 ± 0.24 hours agrees with the accepted transit duration of 1.827 ± 0.029 hours.

The decrease in the flux of HD 189733 after accounting for transit can possibly be explained by the star's variability as a BY Draconis Variable.

We encountered technical difficulties with telescope tracking during our series of observations. We spent approximately 30 minutes to restore the telescope alignment, resulting in an approximately 30-minute break in observations shortly after the transit ended. In addition, our later raw science images registered counts significantly lower than 10,000 counts in the brightest star (our science star) and hence resulted in systematic error in our data by decreasing signal-to-noise ratio. Our target for exposures was approximately 20,000 counts per pixel in the brightest star. We should have increased the exposure time to increase the counts in the brightest star back to 20,000, and hence increase signal-to-noise ratio and reduce systematic error in our flux data. (von der Linden, Anja 2022a)

Approximately 40 of our 600 images (7%) were taken after 01:45, when our target star dipped below 30° altitude. Hence, approximately 7% of our exposures, have additional statistical error in flux measurements.

8. ACKNOWLEDGEMENTS

We thank the Stony Brook University Department of Physics and Astronomy for offering the AST 443 course and providing the equipment used to conduct observations. We thank TAs Ben Levine and Aaron Meuninghoff for providing guidance before and during our observing sessions and feedback regarding our data reduction and analysis. We thank Prof. von der Linden for teaching the AST 443 course and instructing us in the fundamentals of astronomical observation, computing, data analysis, and scientific report writing.

Facilities: Mount Stony Brook Observatory (SBU):14in

Software: astropy (Astropy Collaboration et al. 2013, 2018), Source Extractor (Bertin & Arnouts 1996) SIMBAD (Wenger, M. et al. 2000), Exoplanet.eu, StarAlt (Méndez et al. 2002), AAVSO (aav 2022), DS9 (Joye & Mandel 2003), Cartes du Ciel (Chevalley 2019), Transit Predictor Tool (ipa 2022)

APPENDIX

A. CALCULATIONS

A.1. *Determining target star lightcurve*

For each image i, we calculate the weighted mean of the normalized fluxes (4.1) of reference stars (of index j):

$$\mu_i^{\text{ref}} = \frac{\sum_j f_j^{\text{ref}}/(\sigma_j^{\text{ref}})^2}{\sum_j 1/(\sigma_j^{\text{ref}})^2} \tag{A1}$$

and the error on the weighted mean:

$$\sigma_i^{\text{ref}} = \sqrt{\frac{1}{\sum_j 1/(\sigma_j^{\text{ref}})^2}} \tag{A2}$$

For each image i, we normalize the flux of the target star by the weighted mean flux of the reference stars to obtain r_i:

$$r_i = \frac{f_i^{\text{ref}}}{\mu_i^{\text{ref}}} \tag{A3}$$

and error of r_i:

$$\sigma_{r_i} = r\sqrt{\left(\frac{\sigma_f}{f}\right)^2 + \left(\frac{\sigma_\mu}{\mu}\right)^2} \tag{A4}$$

Next, we calculate the baseline flux of the target star by averaging the normalized fluxes (4.1) before and after the transit. We divide every r_i, σ_{r_i} by this baseline flux and plot the r_i values with error bars with respect to observation time (MJD).

A.2. *Transit depth*

We calculated transit depth from binned data. Given an average pre-transit flux $f_{0,binned}$, post-transit flux $f_{2,binned}$, and during-transit flux $f_{1,binned}$, we calculate transit depth δ as follows:

$$\delta = \frac{1}{2}(f_{0,binned} + f_{2,binned}) - f_{1,binned} \tag{A5}$$

Based on initial uncertainties $\sigma_{f0,binned}, \sigma_{f2,binned}, \sigma_{f1,binned}$ in pre-transit, post-transit, and during-transit flux measurements, respectively, we propagate these uncertainties to determine the uncertainty in the transit depth σ_δ:

$$\sigma_\delta^2 = \frac{1}{4}(\sigma_{f0,binned}^2 + \sigma_{f2,binned}^2) + \sigma_{f2,binned}^2 \tag{A6}$$

A.3. *Planet-to-star radius radio from transit depth*

$$\delta = \frac{R_p^2}{R_*^2} \tag{A7}$$

where R_p is planet radius and R_* is star radius (tra 2020).

Uncertainty in planet-to-star radius ratio $\sigma_{Rp/R*}$ is propagated from uncertainty in transit depth σ_δ as follows:

$$\sigma_{Rp/R*} = \frac{\sigma_\delta}{2\sqrt{\delta}} = \frac{\sigma_\delta}{2(R_p/R_*)} \tag{A8}$$

A.4. *Significance of results*

Given our measurement result $x_1 \pm \sigma_{x_1}$ and the literature value $x_2 \pm \sigma_{x_2}$, we calculate the significance of our result in units of σ: (von der Linden, Anja 2022b)

$$\frac{|x_1 - x_2|}{\sqrt{\sigma_{x_1}^2 + \sigma_{x_2}^2}} \tag{A9}$$

B. SUPPLEMENTARY MATERIAL

Our source code is the Jupyter Notebook file 'Lab 2 - Group Code - FINAL.ipynb'. Our flux tables are the CSV files with filename '4.3_*_time_flux.csv'.

REFERENCES

2020, Transit Algorithms, Caltech. https://exoplanetarchive.ipac.caltech.edu/docs/transit/transit_algorithms.html

2022, Transit Predictor Tool, Caltech. https://www.ipac.caltech.edu/project/transit-predictor-tool

2022, HD 189733, Université de Strasbourg/CNRS. https://simbad.u-strasbg.fr/simbad/sim-basic?Ident=HD%2B189733

2022, Variable Star Plotter, American Association of Variable Star Observers. https://app.aavso.org/vsp/

Astropy Collaboration, Robitaille, T. P., Tollerud, E. J., et al. 2013, A&A, 558, A33, doi: 10.1051/0004-6361/201322068

Astropy Collaboration, Price-Whelan, A. M., Sipőcz, B. M., et al. 2018, AJ, 156, 123, doi: 10.3847/1538-3881/aabc4f

Bertin, E., & Arnouts, S. 1996, A&AS, 117, 393, doi: 10.1051/aas:1996164

Cauley, P. W., Redfield, S., & Jensen, A. G. 2017, The Astronomical Journal, 153, 217, doi: 10.3847/1538-3881/aa6a15

Chevalley, P. 2019, Cartes du Ciel-Skychart. https://www.ap-i.net/skychart//en/start

Joye, W. A., & Mandel, E. 2003, Astronomical Data Analysis Software and Systems XII, ASP Conference Series, 295, 489–492

Méndez, J., Sorensen, P., & Azzaro, M. 2002, Object Visibility - STARALT, Isaac Newton Group of Telescopes. http://catserver.ing.iac.es/staralt/index.php

Sing, D. K., Désert, J.-M., Lecavelier des Etangs, A., et al. 2009, A&A, 505, 891, doi: 10.1051/0004-6361/200912776

von der Linden, Anja. 2022a, Lecture 4: Statistics, part I

—. 2022b, Lecture 5: Statistics part II

—. 2022c, Lecture 2: Time / Flux and magnitudes / Earth's atmosphere

Wenger, M., Ochsenbein, F., Egret, D., et al. 2000, Astron. Astrophys. Suppl. Ser., 143, 9, doi: 10.1051/aas:2000332

Winn, J. N., Holman, M. J., Henry, G. W., et al. 2007, The Astronomical Journal, 133, 1828, doi: 10.1086/512159